Numerical study of two-dimensional generation and collapse of Langmuir solitons

N. R. Pereira and R. N. Sudan

Laboratory of Plasma Studies, Cornell University, Ithaca, New York 14853

J. Denavit

Technological Institute, Northwestern University, Evanston, Illinois 60201
(Received 17 November 1976)

Numerical studies of various aspects of two-dimensional Langmuir solitons, are made, viz., (i) instability and collapse of a planar soliton perturbed in the perpendicular direction, (ii) the effect of an approximate Landau damping on the collapse, and (iii) the generation and subsequent collapse of planar solitons by an external pump field. These computations verify the flow of energy from long wavelength pump fields, through soliton formation and collapse, to shorter wavelengths, where the energy is transferred to the electrons.

I. INTRODUCTION

The theory of strong, electrostatic, plasma turbulence can be developed conceptually, in terms of an ensemble of Langmuir solitons.[1-3] These solitons are strongly nonlinear wavepackets of electrostatic plasma oscillations trapped in self-created density depressions in the background plasma. They are generated by a source of energy at wavelengths long compared with the Debye length λ_D, e.g., an external pump field provided by a powerful laser or the unstable waves generated by beam-plasma interaction. Solitons arise spontaneously, out of the thermal noise, and reach a certain amplitude before they suffer an instability[4-10] which leads to a collapse,[1] i.e., a shrinkage in their physical dimensions accompanied by a corresponding increase in the energy density. When the scale-length approaches λ_D, strong Landau damping follows and the high-frequency wave energy is dissipated into particle energy. Without the pressure exerted by the plasma oscillations the density depressions cannot be maintained in equilibrium and the low-frequency energy is radiated as ion sound waves. Thus, solitons have a finite lifetime in two and three dimensions and steady state is reached only when the rates of production and annihilation balance each other. The growth and decay of solitons provides the physical mechanism for transferring plasma wave energy at long wavelengths to short wavelengths[3] which is absorbed by wave-particle resonances.

In a previous paper,[11] hereafter referred to as (I), a careful comparison has been made of the excitation, propagation, and interaction of solitons in *one* dimension by two different numerical techniques, viz., (i) particle simulation and (ii) a fluid code based on Zakharov's model equations.[1] Our conclusion from (I) is that the results from these two codes are in reasonable agreement provided the effect of electron Landau damping is suitably included in the fluid code.

In the present paper we employ a two-dimensional fluid code to conduct a detailed study of:

(a) The instability of a planar soliton to a two-dimensional perturbation and comparison of the growth rate with analytical predictions.

(b) The long time evolution of this instability which leads to the eventual collapse of the soliton accompanied by the excitation of ion sound waves.

(c) The generation of solitons from random thermal fluctuations by an external pump field close to the electron plasma frequency, and their subsequent collapse.

The situation in two dimensions is notably different from that in one dimension. Because solitons do not collapse in one dimension, the soliton lifetime is very long and equilibrium is achieved by the balance of damping and growth in each individual soliton. Thus, the solitons retain their identity in one dimension[11] whereas they are statistical events in two dimensions.

The model equations for Langmuir turbulence used in this study are Eqs. (6) and (7) of (I) which we repeat here, for convenience, in the same notation and system of dimensionless units.

$$\nabla\cdot(i\partial\mathbf{E}/\partial t+\nabla\nabla\cdot\mathbf{E}-N\mathbf{E})=0\ , \tag{1}$$

$$\partial^2 N/\partial t^2-\nabla^2 N=\nabla^2|\mathbf{E}|^2\ . \tag{2}$$

No stationary solutions of Eqs. (1) and (2) in two dimensions are known except the planar soliton, which in each cross section has the one-dimensional soliton form,[2]

$$E_{x0}=[2(1-v^2)]^{1/2}K\exp[i(\tfrac{1}{2}vx-\Omega t)]/\cosh K(x-vt)\ , \tag{3a}$$

$$\Omega=v^2/4-K^2\ ,$$

$$E_{y0}=0\ , \tag{3b}$$

$$N_0=-2K^2/\cosh^2K(x-vt)=-|E|^2/(1-v^2)\ . \tag{3c}$$

[Note that the symbol K here is equal to k_0 of (I).] However, this solution of Eqs. (1) and (2) is unstable to perturbations in the y direction, which leads to a collapse in finite time of the electric energy density $|\mathbf{E}|^2$ and ion density N.

Two aspects of this collapse have received theoretical attention, viz., (i) the linear growth rate γ of an initial perturbation on the soliton as function of the pa-

 Copyright © 1977 American Institute of Physics

Downloaded 22 Nov 2009 to 132.250.22.8. Redistribution subject to AIP license or copyright; see http://pof.aip.org/pof/copyright.jsp

rameters K, v, and perturbation wavenumber k_y, and (ii) a possible self-similar solution in the collapse stage.

Most analytical studies have concentrated on a modified scalar version of Eq. (1), viz.,

$$i\partial E/\partial t + \partial^2 E/\partial x^2 + \partial^2 E/\partial y^2 - NE = 0 , \tag{4}$$

where $E \equiv E_x$. When ion inertia is neglected in Eq. (2), then $N = -|\mathbf{E}|^2$. With this additional approximation, calculations by Zakharov and Rubenchik[8] and by Yajima[10] on the stability of stationary solitons ($v = 0$) lead to

$$\gamma^2 = 4k_y^2 K^2 , \tag{5}$$

where k_y is the perturbation wavenumber in the y direction. These calculations assume that $k_y/K \ll 1$. When k_y/K is small but finite, Degtyarev *et al.*[7] obtain,

$$\gamma^2 = 4k_y^2 K^2 (1 - k_y^2/4K^2)/(1 + \beta k_y^2/2) , \tag{6}$$

for a standing soliton ($v = 0$), where $\beta = 11.95$ is a combination of integrals over functions connected to Eq. (3a). This calculation indicates a cutoff in growth rate when k_y approaches $2K$. An approximate, but much simpler version of the calculation leading to (5) and (6), is as follows. The perturbation $\delta E(x, t)\exp(ik_y y)$ is determined by the first order equations from (4),

$$[-i\partial/\partial t + \partial^2/\partial x^2 + |E_0|^2 - k_y^2]\,\delta E + |E_0|^2(\delta E + \delta E^*) = 0 , \tag{7a}$$

$$[i\partial/\partial t + \partial^2/\partial x^2 + |E_0|^2 - k_y^2]\,\delta E^* + |E_0|^2(\delta E + \delta E^*) = 0 . \tag{7b}$$

From these equations we obtain

$$i\partial(\delta E + \delta E^*)/\partial t + [\partial^2/\partial x^2 + |E_0|^2 - k_y^2](\delta E^* - \delta E) = 0 , \tag{8a}$$

$$i\partial(\delta E^* - \delta E)/\partial t + [\partial^2/\partial x^2 + 3|E_0|^2 - k_y^2](\delta E + \delta E^*) = 0 . \tag{8b}$$

Combining Eqs. (8a) and (8b) we obtain a fourth-order partial differential equation for $(\delta E + \delta E^*)$,

$$\partial^2/\partial t^2 + [\partial^2/\partial x^2 + |E_0|^2 - k_y^2][\partial^2/\partial x^2 + 3|E_0|^2 - k_y^2](\delta E + \delta E^*) = 0 . \tag{9}$$

Since the original equation, (4), is valid only for $(\partial/\partial x)/k_y \gg 1$, we notice that growing solutions dependent on k_y, are possible only if the variation of δE is determined by

$$(\partial^2/\partial x^2 + |E_0|^2)\delta E \simeq 0 , \tag{10}$$

thus annihilating the dominant terms in the first bracket of (9). We conclude that $\delta E \simeq \epsilon |E(x)| \exp(ik_y y + \gamma t)$ with $\epsilon \ll 1$, and

$$\gamma^2 \simeq 2k_y^2 |E_0|^2 (1 - \tfrac{1}{2} k_y^2/|E_0|^2) . \tag{11}$$

Equation (11) is to be interpreted as valid in the central region of the soliton. We may therefore replace $|E_0|^2$ by $2K^2$ from (3a) and recover the Degtyarev *et al.*[7] result, viz., Eq. (6), except for the small correction given by the denominator.

When the approximation $E_y \ll E_x$ is not made, i.e., we revert to Eq. (1) with $N = -|\mathbf{E}|^2$, Zakharov and Rubenchik[8] obtain for $k_y \ll K$

$$\gamma^2 = 4k_y^2 K^2 \{1 - [3 - \tfrac{7}{4}\zeta(3)]\} \simeq 0.4 k_y^2 K^2 , \tag{12}$$

where ζ is the Riemann zeta function. We see that neglecting E_y results only in a change in the numerical coefficient without affecting the dependence of γ on k_y and K.

Finally, Schmidt[9] has computed the stability of a soliton with arbitrary velocity $v < 1$ including ion inertia and therefore, utilizing Eq. (2). He obtains

$$\gamma^2 = 4|k_y| K^2 [\tfrac{2}{15}(1 - v^2)]^{1/2} , \tag{13}$$

in the limit $k \gg 1 \gg k_y$. However, in the limit $v \to 0$ this result does not agree with the previous derivations, but the reason for this discrepancy is not apparent.

Numerical computations described subsequently in Sec. II approximately confirm the cutoff feature in γ as k_y approaches $2K$ predicted by (6) and (11). The actual temporal evolution of $|\mathbf{E}|^2$ is an even function of time and varies initially as t^2. This follows from the symmetry properties of Eqs. (1) and (2), viz., invariance under space reversal and under time reversal with complex conjugation. If all initial conditions also have these symmetries, then any real function of time or its Taylor series is a function of t^2. Thus, for early times we observe

$$|\mathbf{E}(t)|^2 = |\mathbf{E}(0)|^2 (1 + \Gamma^2 t^2 \cos k_y y) , \tag{14}$$

where $\Gamma \propto \gamma$.

After the linear growth stage, the instability develops into the collapse stage with large local values for the amplitudes. Higher order terms in E and N appear in the equations, so that instead of a completely collapsed state, stationary and oscillatory solutions are possible with large amplitudes.[12] However, these corrections still allow an energy invariant.

Computer solutions of Eqs. (1) and (2), presented in the next section, indicate a quasi-self-similar solution for the electrostatic energy in the collapse stage (see also Refs. 6 and 7). In a self-similar solution, the dependent variable ψ is of the form

$$\psi(\mathbf{x}, t) = f^p(t)\chi(\boldsymbol{\zeta}) , \tag{15}$$

with the coordinate

$$\mathbf{x} = f(t)\boldsymbol{\zeta} . \tag{16}$$

Substituting the form (15) for the potential ψ, with $\mathbf{E} = -\nabla\psi$, and analogously $N = f^q \nu(\boldsymbol{\zeta})$ in Eq. (1), we find that for a self-similar solution

$$f(t) = (t' - t)^{1/2} . \tag{17}$$

From the conservation of total electrostatic energy $W = \int |\mathbf{E}|^2 \, dx\, dy$ we obtain

$$|\mathbf{E}|^2 \propto f^{-2} |\mathbf{E}'(\zeta)|^2 \propto (t' - t)^{-1} |\mathbf{E}'(\zeta)|^2 . \tag{18}$$

For the self-similar ion density ν we find, from Eq. (2),

$$8\nu + 6(\boldsymbol{\zeta} \cdot \nabla_\zeta)\nu + (\boldsymbol{\zeta} \cdot \nabla_\zeta)^2 \nu = 4f^2 \nabla_\zeta^2 (\nu + |\nabla_\zeta \chi|^2) . \tag{19}$$

The right-hand side depends explicitly on time, through

Downloaded 22 Nov 2009 to 132.250.22.8. Redistribution subject to AIP license or copyright; see http://pof.aip.org/pof/copyright.jsp

the function f. In general, a self similar solution cannot be found. However, in the limit $t \to t'$ the right-hand side goes to zero. Then, we can find a radially symmetric solution in arbitrarily scaled coordinates. With ν a function of radius $|\zeta|$ only, we obtain

$$\nu = c|\zeta|^{-2} + d|\zeta|^{-4}, \tag{20}$$

where the constant $d = 0$, because the integrated ion density is invariant. Equation (20) predicts ellipses of arbitrary eccentricity for the level lines.

The model equations, (1) and (2), are not invariant under a scaling[13] of the independent and dependent variables $x' = Kx$, $t' = K^h t$, $N = K^2 N'$, and $E = KE'$. Here, K is an arbitrary constant. The choice of the integer $h = 1$ leaves Eq. (2) invariant, but not Eq. (1), while the choice $h = 2$ leaves Eq. (1) invariant, but not Eq. (2). Thus, solitons with different values of the parameter K can behave qualitatively different, since the relative importance of the time derivative of Eqs. (1) and (2) depends on K. Our choice of K around 2 in the following sections was suggested by the results of (I), obtained with $m_e/m_i = 0.01$, where solitons with K larger than 2 are heavily Landau damped.

II. TWO-DIMENSIONAL INSTABILITY AND COLLAPSE OF A PLANAR SOLITON

In this section we present numerical solutions of the collapse of a planar soliton perturbed in the perpendicular direction. These solutions were obtained using a two-dimensional algorithm based on the spectral representation of Eqs. (1) and (2).[5,11] Periodic boundary conditions are used with periodicity lengths L_x and L_y, corresponding to a discrete spectrum with $\mathbf{k} = (2\pi n_x/L_x)\hat{x} + (2\pi n_y/L_y)\hat{y}$, where n_x and n_y are integers satisfying the condition $(n_x^2 + n_y^2)^{1/2} \le n_{\max}$. Most computations were done with a spatial grid of 32×32 points, corresponding to $n_{\max} = 10$, or 334 modes.

A planar soliton, propagating in the x direction, is initialized with an electric field amplitude defined by Eq. (3) with $t = 0$, and a perturbed ion density defined by

$$N = -(2K^2/\cosh^2 Kx)(1 + 2\epsilon \cos k_y y), \tag{21}$$

where ϵ is the perturbation parameter. The periodicity length in the direction of propagation is $L_x = 6$ in all solutions presented in this section, so that the soliton is free from the boundary of the system. The wavelength of the perturbation is always chosen equal to the periodicity length in the perpendicular direction, i.e., $k_y = 2\pi/L_y$. Table I defines other relevant parameters of the various solutions. Note that no initial perturbation is given to the electric field, or to the derivative of the ion density $\partial N/\partial t$. In most cases the soliton is unstable; however, for short periodicity lengths in the y direction, or for small values of K, initially stable solitons were observed, as noted in Table I.

We examine separately in subsection A the parameter dependence of the initial growth rate of the instability in subsection B, the self-similar character of the solution in the collapse stage, and in subsection C the effect of Landau damping on the soliton collapse.

A. Initial stage of the soliton instability

The initial evolution of the transversely perturbed soliton in run 8 is shown in Fig. 1. At $t = 0.5$ the electrostatic energy, initially unperturbed, is already more concentrated at the original minimum of the ion density ($x = y = 0$). At $t = 1.0$ this concentration is even more pronounced, with the electrostatic energy maximum, $|\mathbf{E}|_m^2$, having increased to twice its initial value at $x = y = 0$, and decreased to 0.6 of its initial value at the boundaries $y = \pm 8$. This condensation of electrostatic energy at $x = y = 0$ is accompanied by a corresponding ion density depletion. The evolution of the energy density maximum, $|\mathbf{E}(t)|_m^2$ at $x = y = 0$, for the solution shown in Fig. 1 is represented in Fig. 2(a) in terms of the increment $\Delta|\mathbf{E}|_m^2 = |\mathbf{E}(t)|_m^2 - |\mathbf{E}(0)|_m^2$. Note that after an initial stage (region 1) corresponding to a rearrangement of the electric field $\mathbf{E}$ in the initial ion density depletion, $\Delta|\mathbf{E}|_m^2$ increases with a quadratic time dependence of the form $\Delta|\mathbf{E}|_m^2 = |\mathbf{E}(0)|_m^2 \Gamma^2 t^2$ (region 2). This quadratic dependence, represented by a linear variation in the plot of Fig. 2(a), is maintained while $\Delta|\mathbf{E}|_m^2$ increases by approximately an order of magnitude. Its rate Γ remains constant out to $t \simeq 0.7$, where the relative change in the maximum $\Delta|\mathbf{E}|_m^2/|\mathbf{E}(0)|_m^2$ reaches 0.16 and the linearization approximation is expected to break down.

The maximum of $|\mathbf{E}|^2$ as a function of y, plotted in Fig. 2(b) for $t = 0.5$ and $t = 1.0$ shows that the perturbation retains a dependence of the form $\cos(k_y y)$ and therefore, grows at approximately the same rate Γ for all values of y, in agreement with Eq. (14).

The growth rate Γ is plotted as a function of the perturbation wavenumber k_y in Fig. 3(a) for a given value $K = 2$ of the soliton parameter. Note that the growth

TABLE I. The parameters of the collapsing planar solitons; L_y is the periodicity length in the y direction, K is the soliton strength parameter, v is the soliton group velocity, and ϵ is the perturbation amplitude. All computations used a periodicity length in the x direction $L_x = 6$.

Run	L_y	K	v	ϵ	Comments
1	4	2	0	0.1	stable
2	4.57	2	0	0.1	stable
3	5.82	2	0	0.1	
4	8	2	0	0.1	
5	12	2	0	0.1	
6	16	2	0	0.025	
7	16	2	0	0.05	
8	16	2	0	0.1	
9	16	1	0	0.1	stable
10	16	4	0	0.1	
11	16	2.387	0	0.1	
12	16	2	0.6	0.1	
13	16	2	0.8	0.1	
14	16	2	0.9	0.1	
15	32	2	0	0.1	
16	64	2	0	0.1	
17	8	2	0	0.1	Landau damping

Downloaded 22 Nov 2009 to 132.250.22.8. Redistribution subject to AIP license or copyright; see http://pof.aip.org/pof/copyright.jsp

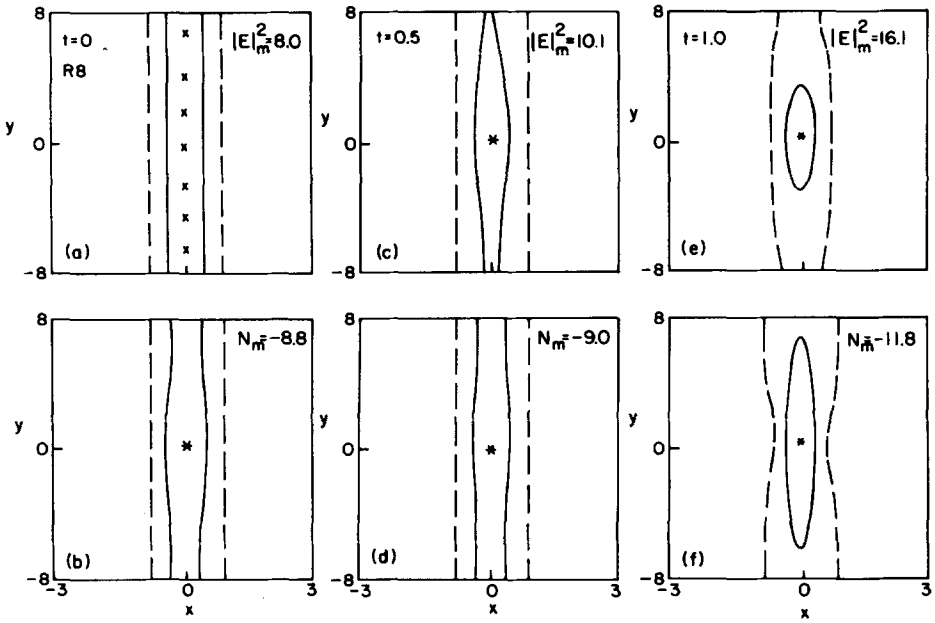

FIG. 1. The electrostatic energy $|\mathbf{E}|^2(x, y, t)$ and the ion density perturbation $N(x, y, t)$ for run 8. The solid lines are the level lines at 0.5 of the maximum, the broken lines at 0.1 of the maximum. The asterisk indicates the position of the maximum value.

rate drops for wavenumbers k_y of the order of a representative wavenumber $k_x \simeq 1.2$ in the direction of propagation. Figure 3(b) shows the growth rate as a function of the parameter K for a given value $k_y = 2\pi/16$

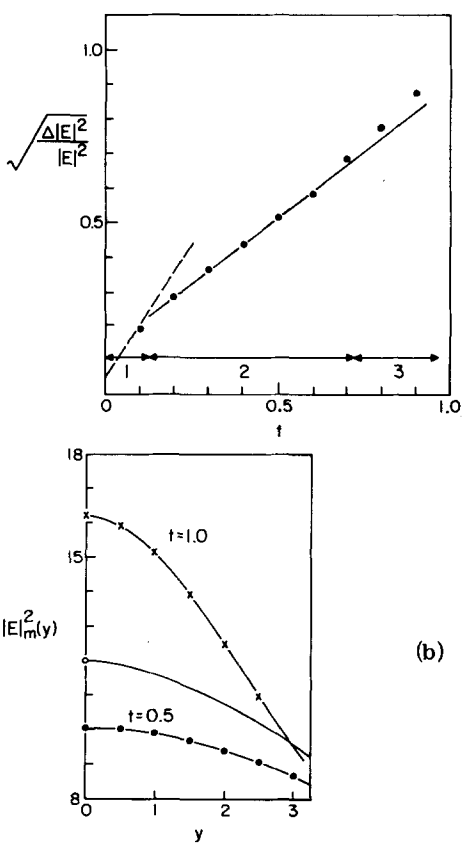

FIG. 2. (a) The square root of the relative change in the maximum of the electrostatic energy density as a function of time. The slope of the solid line is the growth rate Γ. The fast growth for small times is indicated by the broken line. (b) The electrostatic energy density at $x = 0$, as a function of y, for time $t = 0.5$ (dots) and $t = 1.0$ (crosses). The solid line is the function $4\cos k_y y$.

of the perturbation wavenumber. The logarithm of the growth rate is plotted versus the logarithm of K and the straight line, which fits the data points for $1.5 < K < 3.5$ indicates a dependence of the form $\Gamma \propto K^2$.

The evolution of the ion density for the solution shown in Fig. 1 is given in Fig. 4. In Fig. 4(a), the ion density minimum $N_m(t)$ is represented in terms of the decrement $\Delta N = N_{m0} - N_m(t)$, where $N_{m0} = -|\mathbf{E}(0)|^2_m$ denotes the unperturbed ion density minimum. For $t < 0.3$, i.e., during the initial stage which corresponds to a redistribution of the electrostatic energy in the density depression, the depth of the density depression decreases, giving negative values of ΔN having an initial quadratic time dependence, $\Delta N \propto -t^2$. This initial time dependence is evident in the lower part of Fig. 4(a) where the circles represent values of $(-\Delta N/|N|)^{1/2}$, which exhibits an initial linear time dependence. After the initial stage, the instability causes the density depression to increase, giving positive values of ΔN having a time dependence now of the form $\Delta N \propto t^4$. This time dependence is evident in the upper part of Fig. 4(b)

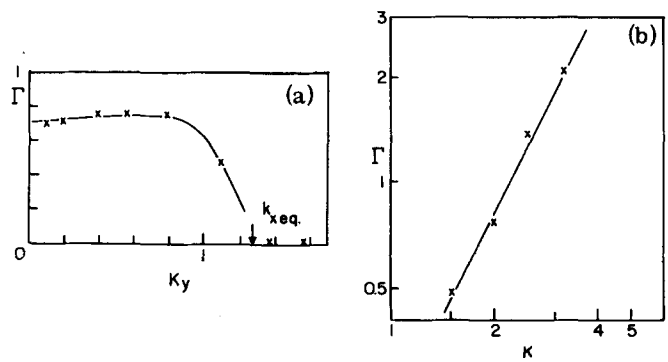

FIG. 3. (a) The growth rate Γ as a function of k_y. The wavenumber corresponding to the half-width of the spectrum of the soliton in the x direction is given by the arrow. (b) The logarithm of the growth rate Γ versus the logarithm of the strength parameter K. The solid line corresponds to $\Gamma \propto K^2$.

Downloaded 22 Nov 2009 to 132.250.22.8. Redistribution subject to AIP license or copyright; see http://pof.aip.org/pof/copyright.jsp

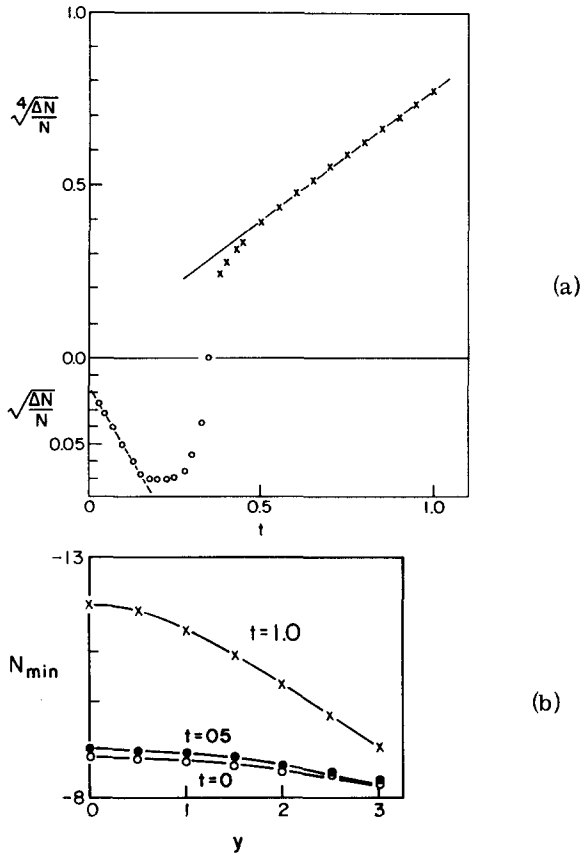

FIG. 4. Growth of the minimum of the ion density as a function of time for run 8. (a) The square root of the relative change of the minimum of $N(x,y,t)$ for $t<0.35$ (open circles), and the fourth root of the relative change for $t>0.35$ (crosses). The broken line indicates the initial decay with t^2, the solid line the later growth proportional to t^4. (b) The minimum of the ion density at $x=0$ as a function of y, for time $t=0.0$ (open circles), $t=0.5$ (dots) and $t=1.0$ (crosses).

where the crosses represent values of $(\Delta N/|N|)^{1/4}$, which exhibits a linear time dependence for $t \gtrsim 0.5$. The density minimum (at $x=0$), plotted versus y in Fig. 4(b) for $t=0$, 0.5 and 1.0, shows that the ion density perturbation retains a dependence of the form $\cos(k_y y)$.

These computations were concerned with the instability of a standing soliton, i.e., $v=0$. The evolution of a moving soliton, with $v=0.6$, Eq. (3), is given in Fig. 5 at $t=1.5$. The initially planar soliton is observed to have accelerated in the x direction for $|y|>4$, where the electrostatic energy decreases, while in the central region, $|y|<4$, where the electrostatic energy increases, the soliton has decelerated. In Fig. 5 the contour plot of the perturbed soliton may be compared with the arrows located at $x=vt=0.9$, which correspond to the location of the maximum of an unperturbed soliton. The connection between the soliton group velocity and its local electrostatic energy observed here, was also seen for one-dimensional solitons in (I) where the decrease in energy density was due to Landau damping. Here, the change in energy density is due to the soliton instability.

Apart from the change in velocity, the collapse occurs as in the case of a standing soliton, with a relative growth rate Γ nearly independent of the velocity.[14] However, since the initial energy density maximum $|\mathbf{E}(0)|_m^2$ is proportional to $1-v^2$, the energy increment $\Delta|\mathbf{E}|_m^2$, for given values of K and k_y, grows at a slower rate as v increases. In this sense, solitons become less unstable as their group velocity increases.[5]

We note that the results of Figs. 3(a) and 3(b) are in apparent conflict with the theoretical results of Eqs. (5)–(6) and (11)–(13). While we do not expect accurate quantitative agreement between the analytical and computer rates, we should expect the same parameter dependence on k_y and K. We observe a weak dependence of Γ on k_y for $k_y<k_x$, in contrast to the linear dependence of Eqs. (5)–(6) and (12)–(13), and a proportionality to K^2 instead of K. Moreover, after a transient stage, the growth of the ion density perturbation found in Fig. 5(a) is proportional to t^4, instead of having the same dependence (proportional to t^2) as the energy density.

These differences may be attributed to differences between the initial conditions of the numerical solutions, defined by Eq. (21), and the eigenfunctions assumed in theoretical treatments of the instability. Thus, because of the relatively short time over which the soliton collapses in numerical solutions, the perturbation may never acquire the form of a pure mode to which Eqs. (5)–(6) and (11)–(13) apply.

A calculation given in the Appendix and valid only for short times gives the initial growth rate of a perturbation described exactly by Eq. (21) to be

$$\Gamma^2 = 8\epsilon K^4 . \tag{22}$$

This result agrees with the k_y and K dependence of the numerical computations for the range $k_y \ll K$, but is a factor of 3 too large. Moreover, (22) does not predict the decrease in growth rate as k_y approaches K because

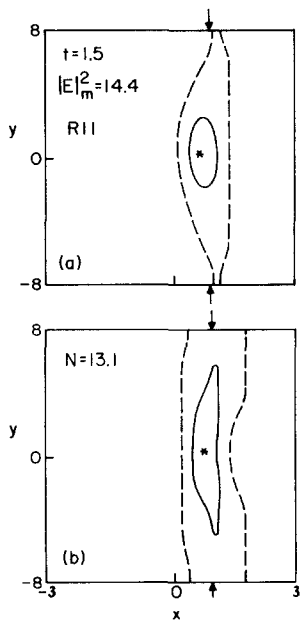

FIG. 5. (a) The electrostatic energy density for a collapsing soliton with group velocity $v=0.6$ at $t=2.0$. (b) The ion density perturbation in this case.

Downloaded 22 Nov 2009 to 132.250.22.8. Redistribution subject to AIP license or copyright; see http://pof.aip.org/pof/copyright.jsp

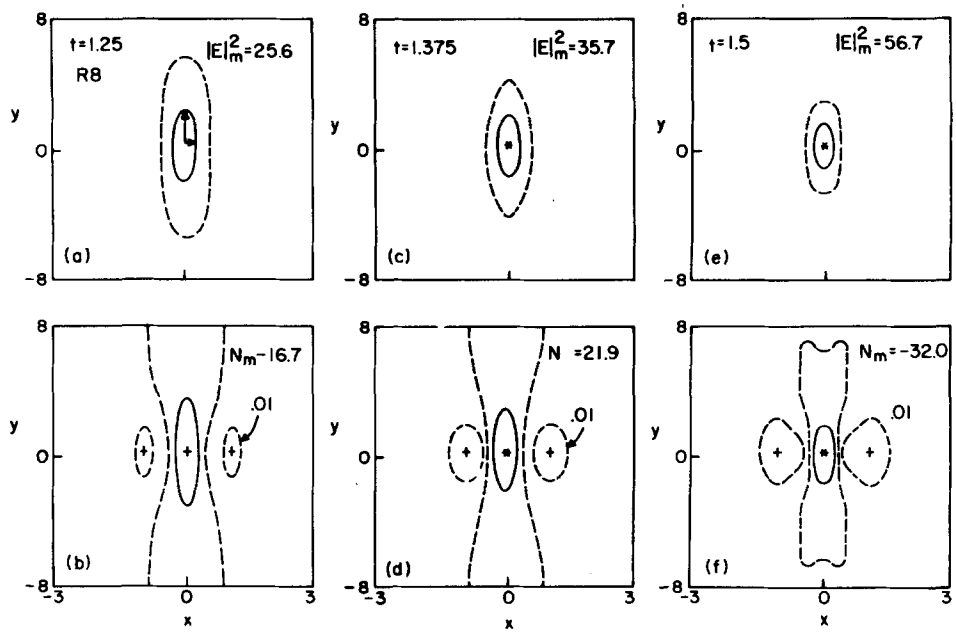

FIG. 6. The electrostatic energy $|\mathbf{E}|^2(x,y,t)$ and the ion density perturbation $N(x,y,t)$ in the collapse stage of run 8. This figure is a continuation of Fig. 1. Positive and negative regions in the plot for $N(x,y,t)$ are indicated by + and −, respectively. Note that the ion density is expelled from the collapsing region.

in the derivation $\mathbf{E}$ was treated as predominantly a scalar quantity. However the cutoff suggested by Eqs. (6) and (11) is in substantial agreement with the numerical results. We also note that the behavior of the density perturbation illustrated in Fig. 4(a) is in substantial agreement with the result given in the Appendix.

B. Final collapse stage

We now consider the final stage of the soliton collapse in which the possibility of a self-similar solution described by Eqs. (15)–(17) has been proposed.[1,6]

The evolution of the electrostatic energy and of the ion density for run 8 during the collapse stage, $1.25 \leq t \leq 1.5$ is shown in Fig. 6. At $t = 1.25$ the level line of $|\mathbf{E}|^2$ at 0.5 of the maximum [solid line in Fig. 6(a)] has assumed an approximately elliptical shape, with axes of half-lengths D_x and D_y indicated by arrows. The level line at 0.1 of the maximum (broken line) is also approximately elliptical. The same is true of the level line at 0.5 of the maximum ion density depletion [solid line in Fig. 6(b)] but not of the level line at 0.1 (broken line). At $t = 1.375$ the level lines of $|\mathbf{E}|^2$ and N are still approximately elliptical, but the shape of the ellipses has changed. This is also true at $t = 1.5$. At all times in this collapse stage there is expulsion of ion density accompanied by condensation of electric field energy in the central region.

To examine the self-similarity of the solution, the maximum of the electrostatic energy is plotted as a function of time before collapse time at $t' = 1.77$ in Fig. 7(a). This collapse time was found by varying t' to obtain the best fit of the data points along a straight line in the double logarithmic scale of Fig. 7(a). However, the slope of this line gives a power law of the form $|\mathbf{E}|^2 \propto |t' - t|^{-1.2}$ instead of the linear dependence implied by Eq. (17). Other solutions with different values of the initial parameter K and perturbation wavenumber k_y show that these quantities do not influence the self-similar behavior strongly.

The half-lengths D_x and D_y of the level line at 0.5 of the maximum of $|\mathbf{E}|^2$ are plotted in Fig. 7(b) using the same collapse time $t' = 1.77$. These plots show that D_x and D_y also follow, approximately, power laws of the form $D_x \propto (t' - t)^{0.4}$ and $D_y \propto (t' - t)^{0.8}$. These power laws are consistent with conservation of total electrostatic energy W, but differ from the power law of Eq. (17) which implies equal powers 0.5 for D_x and D_y. Thus, the present numerical solutions suggest that the assumption of self-similarity must be modified to allow different scales in the x and y directions.

The behavior of the ion density during the collapse stage, and the appearance of regions of excess ion density observed in Fig. 6, can be understood qualitatively as follows. The electrostatic energy density $|\mathbf{E}|^2$ contracts rapidly in the central region, increasing the pon-

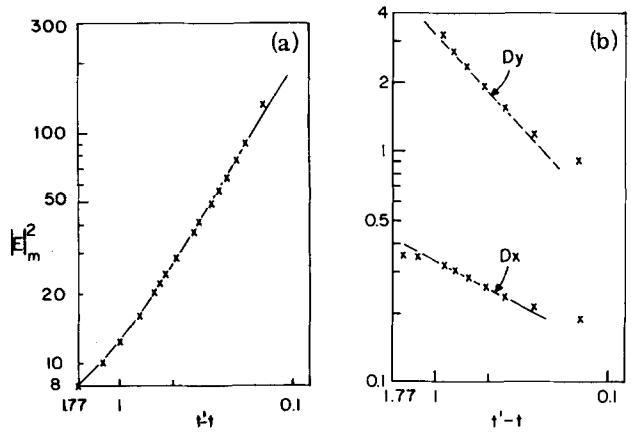

FIG. 7. (a) The maximum of the electrostatic energy density as a function of the time interval to the collpase time t' in the standard case. The line with slope 1.2 fits the data with the choice $t' = 1.77$. (b) The axes of the elliptical level line at 0.5, D_x and D_y, as a function of the distance to the collapse time. The line with slope 0.4 fits the data points for D_x, and the line with slope 0.8 fits the points for D_y.

Downloaded 22 Nov 2009 to 132.250.22.8. Redistribution subject to AIP license or copyright; see http://pof.aip.org/pof/copyright.jsp

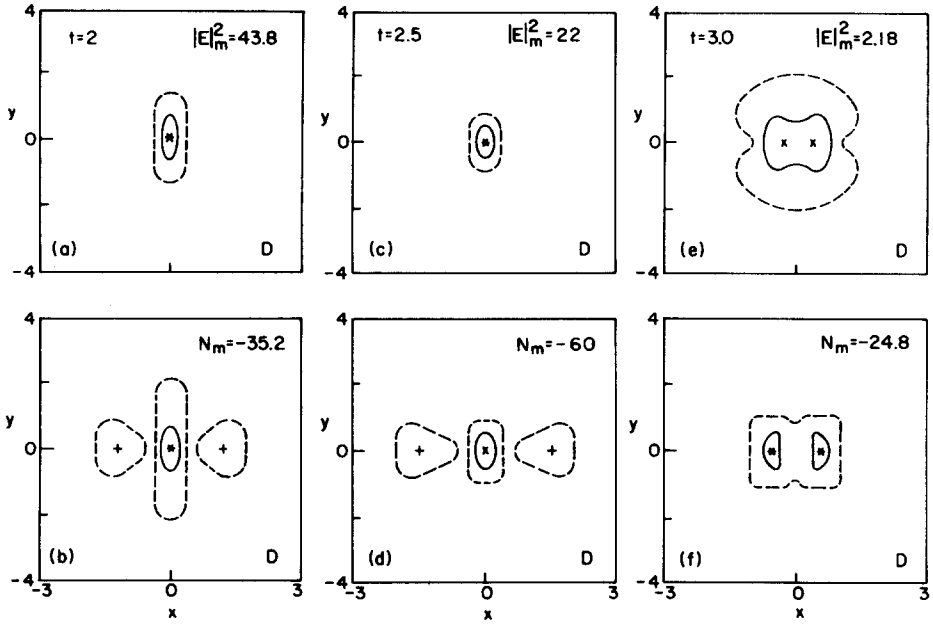

FIG. 8. The electrostatic energy density $|\mathbf{E}|^2(x,y,t)$ and the ion density perturbation $N(x,y,t)$ for the collapse with Landau damping, of run 4. The solid line is the level line at 0.5 of the maximum for the energy density, and at 0.5 of the minimum for the ion density, which are given in the figure. The broken line is the level line at 0.1 of the maximum or minimum. The broken line around the + sign, which indicates a positive region, is at 0.01 of the minimum.

deromotive force and expelling ions form this region. This causes the large ion depletion observed in the central region. However, the regions adjacent to the central region, where electrostatic energy density has decreased, can only partially make room for the expelled ions, since the maximum velocity of propagation of an ion density perturbation is the ion sound speed equal to unity. This sets an outer bound to the region that can be reached by an ion density perturbation at any given time. An estimate of the width of the region of excess ion density is given by the maximum velocity (unity) multiplied by the time Δt during which the self-similar solution is applicable to the central region. In the present case this time is $\Delta t \simeq 1.0$, giving an estimated width of order unity. The width of the region of excess ion density in Fig. 6, approximately 0.8, agrees with the above estimate.

The self-similarly of the solution during the collapse stage is of mathematical interest in establishing solutions of Eqs. (1) and (2), but its physical significance is limited by Landau damping of the Langmuir waves which strongly modifies the collapse stage.

C. Effect of Landau damping on the collapse stage

The effect of resonant particle interactions is included in the present model by introducing damping terms corresponding to Landau damping in the spectral representation of Eq. (1). Comparisons of one-dimensional solutions of the model equations with particle simulations in (I), have shown that the introduction of such terms gives a proper representation of resonant particle interactions.

Landau damping is a function of $k\lambda_D = 2(m_e/m_i)^{1/2}\bar{k}/3$, where k in this expression is in physical units, while $\bar{k}$ denotes the dimensionless wavenumber. For small k, ($k\lambda_D < 0.2$) Landau damping is small, but fields with large gradients, which are generated in the collapse stage correspond to large values of k and are heavily damped. In the computations presented here, a mass ratio $m_e/m_i = 0.01$ has been chosen to allow Landau damping to become significant at an earlier stage of the collapse than it would with a realistic mass ratio, which would necessitate a prohibitively expensive mesh size.

The evolution of the energy density $|\mathbf{E}|^2$ and of the ion density perturbation N in run 17 is shown in Fig. 8. A grid corresponding to 1426 modes was used in this computation. The initial stage of the instability ($t<2$) is not strongly modified by Landau damping and is omitted from Fig. 8. At $t=2$ a strong condensation of energy accompanied by ion density depletion has occurred in the central region. Regions of positive ion density perturbation also appear as in the solution without damping shown in Fig. 6. At $t=2.5$, the maximum of $|\mathbf{E}|^2$ has decreased rather than increased, while the width of the collapse region in the y direction also decreases, unlike the width in the x direction, which remains constant. However, the ion density depletion $-N_m$ continues to increase in this time interval and this large depression in the background plasma keeps $|\mathbf{E}|^2$ concentrated.

When much of the electrostatic energy density, and with it the ponderomotive force, has disappeared due to Landau damping ($t=3$), the ion density perturbation propagates away from the collapse region, and moves out in the original direction of propagation (x direction), dragging what is left of $|\mathbf{E}|^2$ with it. At $t=4$ (not shown), $|\mathbf{E}|^2$ is still contained by the density wells going out in the x direction. Also a smaller circular ion wave, and some wall effects, are evident at that time.

The maximum of $|\mathbf{E}|^2$ and the total electrostatic energy W in this solution are plotted in Figs. 9(a) and 9(b), as functions of time. Initially, $|\mathbf{E}|^2_m$ increases more slowly, but in a similar way as in collapse without damping. At $t=2$ the damping begins to remove energy but the continuing collapse in the y direction maintains the increase in $|\mathbf{E}|^2_m$ until $t=2.2$. The collapse region reaches its minimum extension at $t=2.5$, and W

Downloaded 22 Nov 2009 to 132.250.22.8. Redistribution subject to AIP license or copyright; see http://pof.aip.org/pof/copyright.jsp

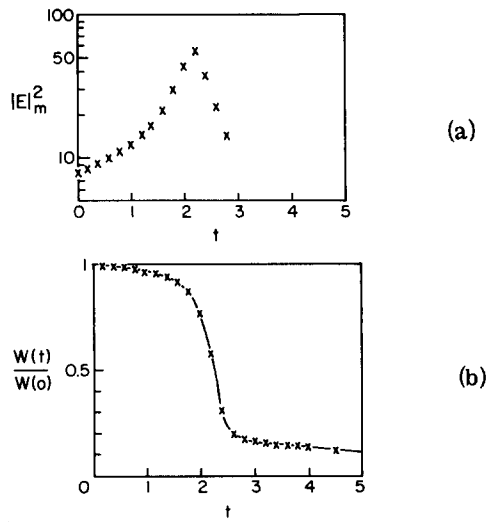

FIG. 9. (a) The maximum of the electrostatic energy density as a function of time for the soliton collapse with Landau damping of Fig. 8. (b) The total electrostatic energy $W(t)$ normalized to $W(0)$ as a function of time. Note the rapid decrease of W for $2<t<3$.

decreases in the same manner as $|\mathbf{E}|^2_m$ between $t=2.5$ and $t=3$. For longer times the wavelengths of the Langmuir oscillations increase, and the damping rate of W returns to its initial small value.

Our computations seem in qualitative agreement with particle simulations of resonant absorption,[15] which follow a mathematical model similar to Eqs. (1) and (2). We have not addressed ourselves to the development of the electron distribution function[16] as a result of the Landau damping, nor have we considered changes in the damping[17] rate coming from a non-Maxwellian electron distribution function. We have observed in (I) that at least in one dimension these corrections do not change the qualitative behavior of the solutions.

III. GENERATION AND COLLAPSE OF TWO-DIMENSIONAL SOLITONS DRIVEN BY AN EXTERNAL PUMP FIELD

Numerical solutions of the generation of soliton-like structures in one dimension from random initial fluctuations by an homogeneous external pump field, have been presented in (I). Soliton generation in two dimensions may be studied numerically in a similar manner, by writing the total electric field amplitude in Eqs. (1) and (2) as $\mathbf{E}(x,y,t)+E_0\hat{x}$, where $\mathbf{E}(x,y,t)$ now denotes the internal field amplitude and E_0 is the constant amplitude of a pump field in the x direction, oscillating at the plasma frequency ω_e. A numerical solution showing two-dimensional soliton generation using this method is illustrated in Fig. 10. This computation, performed on a grid corresponding to 1426 modes, was initialized by setting $N=\partial N/\partial t=0$ and by giving to all electric field modes equal amplitudes $|\mathbf{E}_k|=0.01$ with random phases. The normalized amplitude of the pump field, $\eta=eE_0/m_e\omega_e v_e$, where v_e, is the electron thermal velocity, was chosen as $\eta=0.3$. A system with periodicity length $L_x=L_y=8$ was chosen and Landau damping is included with a mass ratio $m_e/m_i=0.01$.

After a transient period in which the energy W decreases as the higher modes are damped W increases exponentially with the linear growth rate, and at $t=5.5$ a planar soliton-like structure of Figs. 10(a) and (b) is generated. We note that the maximum value $|\mathbf{E}|^2_m$ is larger than $-N_m$, unlike the ideal soliton with zero velocity. After this generating phase, the soliton col-

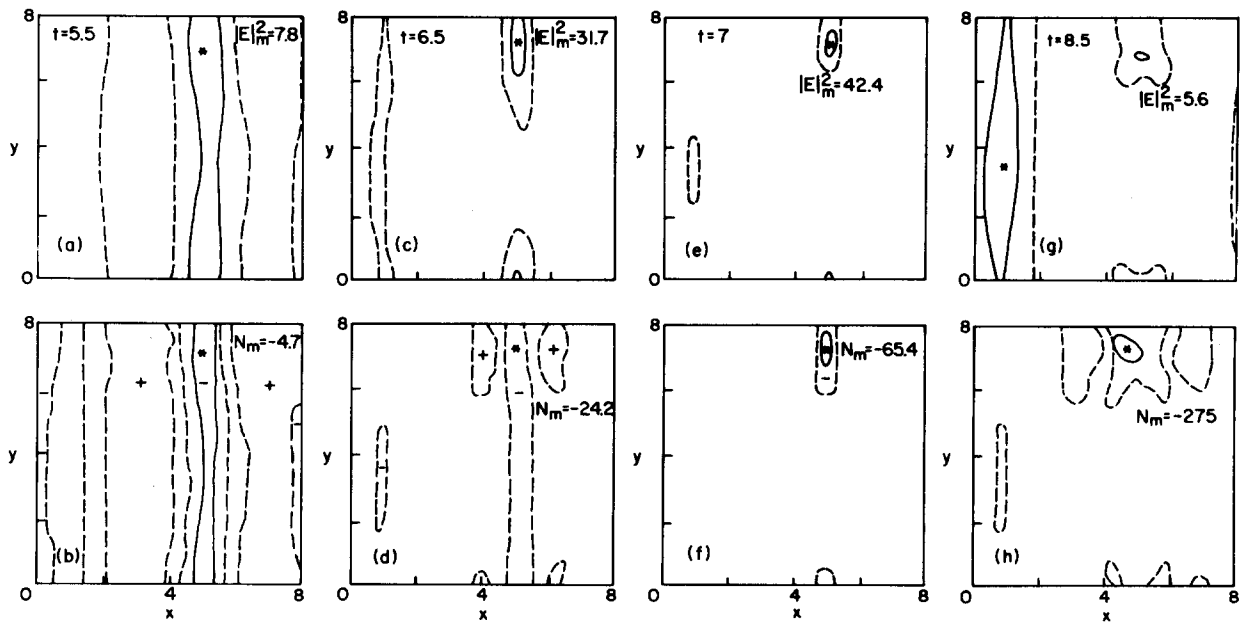

FIG. 10. The electrostatic energy density $|\mathbf{E}|^2(x,y,t)$ and the ion density perturbation $N(x,y,t)$ for the computation driven by an external pump with $\eta=0.3$. The solid line is the level line of 0.5 of the maximum for the energy density $|\mathbf{E}|^2_m$ and at 0.5 of the minimum for the ion density perturbation N_m. The broken line is the level line at 0.1 of the maximum or minimum. The asterisk indicates the position of the maximum value. Positive and negative regions in the plot for $N(x,y,t)$ are indicated by + and −, respectively.

Downloaded 22 Nov 2009 to 132.250.22.8. Redistribution subject to AIP license or copyright; see http://pof.aip.org/pof/copyright.jsp

lapses as shown in Figs. 10(c)–(f), qualitatively in the same manner as the ideal soliton of Fig. 6. The values of the maximum of $|\mathbf{E}|^2$ and of $-N$ increase rapidly, the spatial extent of the collapse region decreases, and ion waves are created. Note that the ion density minimum, which in absolute value is less than $|\mathbf{E}|^2_m$ at $t = 6.5$, reaches a larger value than $|\mathbf{E}|^2_m$ at $t = 7$. This reflects the damping of the electric field as well as the dynamical behavior of N under influence of the ponderomotive force. At $t = 8.5$ most of the electrostatic energy in the collapse region has been absorbed by Landau damping and another soliton-like structure becomes visible at the left in Fig. 10(g), while the ion density perturbation, not accompanied by electrostatic energy, starts to move away from the collapse region in the form of ion waves.

These and other[14] computations with different pump field strengths, periodicity lengths, and mass ratios show that it is not possible to generate stable "blobs" of electrostatic energy in our model in two dimensions, in contrast to soliton generation in one dimension.[11]

In two dimensions, the collapsing electrostatic energy forms an ion density depletion, but the concentration of $|\mathbf{E}|^2$ becomes so large that Landau damping removes most of the energy. Now, the final state consists mostly of ion density waves, but with very little electrostatic energy.

IV. CONCLUSIONS

The present study confirms and extends earlier computations[5] showing the instability and collapse of Langmuir solitons in two dimensions. Additional computations[14] have verified that the essential features of this instability and collapse are not modified by the inclusion of the third dimension.

In contrast to the one-dimensional case, the interaction between the electrostatic energy of Langmuir waves and ion density fluctuations in multi-dimensional situations does not yield stable soliton structures, but generates transient structures which collapse, producing large energy density gradients. The generation of such structures with their subsequent collapse and absorption by Landau damping have been simulated in two dimensions. These computations show that, under the action of an external pump field at the plasma frequency, intense "blobs" of condensed electrostatic energy are continuously created at random, and disappear by Landau absorption. These blobs while not coherent solitons do maintain the approximate amplitude-width relationship of solitons during their lifetime. Thus, the interaction of Langmuir waves with ion density fluctuations in multi-dimensional situations generates a turbulent state of the plasma, rather than the approximately coherent soliton structures found in one-dimensional simulations.[11] This turbulent state is characterized by short wavelengths, whose energy is readily transferred to the particles by Landau absorption.

Note added in proof. As this paper was going to press we were made aware of similar work by Y. S. Sigov and Y. V. Khodirev.

ACKNOWLEDGMENTS

The computations were performed at the National Magnetic Fusion Energy Computing Center, Livermore, California.

This work was supported by the U. S. Energy Research and Development Administration under contracts EY-76-S-02-3170.*000 and EY-76-S-02.2200*000.

APPENDIX

We calculate the instability of the planar soliton (3) as an initial value problem. The electric field is expressed in the form

$$E_x(x, y, t) = E(x) \exp[iS(x, y, t) + iK^2 t] , \tag{A1}$$

where $E(x)$ is the stationary soliton of Eq. (3a), with $v = 0$, and the y component of E is neglected. For the initial ion density, we take Eq. (18) and set $\partial N/\partial t = 0$ at $t = 0$.

Substitution of (A1) in Eq. (4), linearizing and neglecting y derivatives yields, in the neighborhood of $x = 0$

$$\partial S/\partial t = i(\partial^2 S/\partial x^2) - N_1 . \tag{A2}$$

To determine the imaginary part of S we integrate Eq. (A2) twice, assuming that the ion perturbation, N_1, is known. N_1 develops according to

$$\frac{\partial^2 N_1}{\partial t^2} - \frac{\partial^2 N_1}{\partial x^2} = \frac{\partial^2}{\partial x^2} \{|\mathbf{E}|^2(x)\, 2\,\mathrm{Im}[S(x, y, t)]\} , \tag{A3}$$

obtained by linearizing Eq. (2).

Equations (A2) and (A3) can be solved approximately by a series development in time, restricting us to the calculation of an initial growth rate. The first approximation for N_1 follows from the solution of the wave equation (A3), and the initial condition $S = 0$:

$$N_1(x, y, t) = \tfrac{1}{2}[N_1(x - t, y, 0) + N_1(x + t, y, 0)] . \tag{A4}$$

Substituting (A4) in (A2) we find, as a first approximation S_1 to S, the real quantity

$$S_1(x, y, t) = \int_0^t N_1(x, y, t')\, dt' , \tag{A5}$$

which does not change the right-hand side of Eq. (A3). Thus, we can use the same ion density N_1 as previously for the second approximation S_2. Substituting S_1 in the right-hand side of Eq. (A2), making use of the x derivative of (A5) and the special form of the argument of N_I, which allows us to interchange time and space derivatives, we find, for S near $x = 0$,

$$S_2(x, y, t) = S_1(x, y, t) + (i/2)\{2N_1(0, y, 0) - [N_1(x - t, y, 0) + N_1(x + t, y, 0)]\} . \tag{A6}$$

The electrostatic energy at $x = 0$ is now

$$|\mathbf{E}|^2 = |E|^2(t = 0) \times \exp(-\{2N_1(0, y, 0) - [N_1(-t, y, 0) + N_1(t, y, 0)]\}) . \tag{A7}$$

We recognize in the exponent the second differential with respect to time, which is equivalent to the second differential with respect to space, as the right-hand

Downloaded 22 Nov 2009 to 132.250.22.8. Redistribution subject to AIP license or copyright; see http://pof.aip.org/pof/copyright.jsp

side of Eq. (A3) is approximately zero.

A power series development of N around $x=0$ yields

$$|\mathbf{E}|^2 = |\mathbf{E}|^2(t=0)(1+8\epsilon K^4 t^2 \cos k_y y) , \tag{A8}$$

from which we conclude that

$$\Gamma^2 = 8\epsilon K^4 . \tag{A9}$$

In Fig. 2 we have seen that the initial growth develops in two stages. This calculation is strictly valid only in the first stage, which is a re-arrangement of the electrostatic energy in the perturbed potential well formed by the ion density. In the second stage the y derivatives are no longer negligible.

The time development of the ion density is described for small times by Eq. (A4). A power series expansion in time of (A4) shows a decrease of N_1 proportional to t^2. For later times, when the electrostatic energy $|\mathbf{E}|^2$ has grown appreciably, the ion density is expected to evolve mainly under the influence of $|\mathbf{E}|^2$. Then, the x derivative of N in Eq. (2) can be neglected. Using Eq. (A8) we find for N_1

$$N_1(x, y, t) = \int_0^t dt' \int_0^{t'} dt'' \left(\frac{\partial^2}{\partial x^2} |\mathbf{E}|^2\right)_{x=0} = \frac{32}{12} K^8 t^4 \cos k_y y , \tag{A10}$$

indicating a behavior like t^4 at $x=0$, after the initial decay stage proportional to t^2. Equation (A10) is reliable only in terms of the functional form, but not for its numerical value, since the growth rate of the electrostatic energy, Eq. (A9), is only valid up to a constant. The computations presented in Sec. II indeed confirm the time dependence for the ion density N [see Fig. 4(a)].

[1] V. E. Zakharov, Zh. Eksp. Teor. Fiz. **62**, 1745 (1972) [Sov. Phys.-JETP **35**, 908 (1972)].
[2] L. I. Rudakov, Dokl. Akad. Nauk. SSR **207**, 821 (1972) [Sov. Phys.-Dokl. **17**, 1166 (1973)].
[3] A. S. Kingsep, L. I. Rudakov, and R. N. Sudan, Phys. Rev. Lett. **31**, 1482 (1973).
[4] L. M. Degtyarev, V. G. Makhankov, and L. I. Rudakov, Zh. Eksp. Teor. Fiz. **67**, 533 (1974) [Sov. Phys.-JETP **40**, 264 (1975)].
[5] J. Denavit, N. R. Pereira, and R. N. Sudan, Phys. Rev. Lett. **33**, 1435 (1974).
[6] L. M. Degtyarev and V. E. Zakharov, Zh. Eksp. Teor. Fiz. Pis'ma Red. **21**, 9 (1975) [JETP Lett. **21**, 4 (1975)], V. E. Zakharov and V. S. Sinakh, Zh. Eksp. Teor. Fiz. **68**, 940 (1975), and references therein.
[7] L. M. Degtyarev, V. E. Zakharov, and L. I. Rudakov, Zh. Eksp. Teor. Fiz. **68**, 115 (1975) [Sov. Phys.-JETP **41**, 57 (1976)].
[8] V. E. Zakharov and A. M. Rubenchik, Zh. Eksp. Teor. Fiz. **65**, 997 (1973) [Sov. Phys.-JETP **38**, 494 (1974)].
[9] G. Schmidt, Phys. Rev. Lett. **34**, 724 (1975).
[10] N. Yajima, Prog. Theor. Phys. Jpn. **52**, 1066 (1974).
[11] N. R. Pereira, R. N. Sudan, and J. Denavit, Phys. Fluids, 20, 271 (1977); and Bull. Am. Phys. Soc. **19**, 893 (1974); see also G. J. Morales and Y. C. Lee. Phys. Fluids **19**, 690 (1976).
[12] C. E. Max, Phys. Fluids **19**, 74 (1976).
[13] N. Pereira, J. Math. Phys. **17**, 1004 (1976).
[14] N. Pereira, Ph.D. thesis, Cornell University (1976).
[15] K. G. Estabrook, E. J. Valeo, and W. L. Kruer, Phys. Fluids **18**, 1151 (1975).
[16] G. J. Morales and Y. C. Lee, Phys. Rev. Lett. **33**, 1534 (1974); W. M. Manheimer and K. Papadopoulos, Phys. Fluids **18**, 1397 (1975).
[17] J. J. Thomson, R. J. Faehl, W. L. Kruer, and S. Bodner, Phys. Fluids **17**, 937 (1974).

Downloaded 22 Nov 2009 to 132.250.22.8. Redistribution subject to AIP license or copyright; see http://pof.aip.org/pof/copyright.jsp